Proceedings of the 12th International Conference on Low Energy Antiproton Physics (LEAP2016)
Downloaded from journals.jps.jp by 128.141.46.241 on 03/21/18

Proc. 12th Int. Conf. Low Energy Antiproton Physics (LEAP2016)
JPS Conf. Proc. **18**, 011038 (2017)
https://doi.org/10.7566/JPSCP.18.011038

The development of the antihydrogen beam detector: toward the three dimensional tracking with a BGO crystal and a hodoscope

Y. Nagata[1,2], N. Kuroda[3], C. Sauerzopf[4], B. Kolbinger[4], C. Malbrunot[5,4], A. A. Capon[4], P. Dupre[2], B. Radics[2], M. Tajima[3,2], C. Kaga[6], M. Leali[7], E. Lodi Rizzini[7], V. Mascagna[7], O. Massiczek[4], T. Matsudate[3], M. C. Simon[4], H. Breuker[5], H. Higaki[6], Y. Kanai[2], Y. Matsuda[3], L. Venturelli[7], E. Widmann[4], Y. Yamazaki[2]

[1]*Department of Applied Physics, Tokyo University of Agriculture and Technology, Koganei, Tokyo 184-8588, Japan*
[2]*Atomic physics research unit, RIKEN, Wako, Saitama 351-0198, Japan*
[3]*Graduate School of Arts and Sciences, The University of Tokyo, Komaba, Meguro, Tokyo 153-8902, Japan*
[4]*Stefan Meyer Institute for Subatomic Physics, Boltzmanngasse 3,1090 Vienna, Austria*
[5]*CERN, 1211 Geneva 23, Switzerland*
[6]*Graduate School of Advanced Sciences of Matter, Hiroshima University, Higashi-Hiroshima, Hiroshima 739-8530 Japan*
[7]*Dipartimento di Ingegneria dell'Informazione, Università di Brescia & Istituto Nazionale di Fisica Nucleare, Gruppo Collegato di Brescia, 25133 Brescia, Italy*

E-mail: ynagata@cc.tuat.ac.jp

(Received June 15, 2016)

We developed an antihydrogen beam detector for the microwave spectroscopy of the antihydrogen hyperfine splitting. The detector consists of a position sensitive BGO calorimeter and a hodoscope. We report test experiments for the position sensitive readout from a non-segmented BGO crystal.

KEYWORDS: Antihydrogen, Detector, Scintillator

1. Introduction

Syntheses and manipulations of antihydrogen ($\bar{H}$) atoms have been studied extensively in order to perform the CPT symmetry test or the study on the gravitational interaction of antimatter and matter (the earth). Several groups proposed the CPT test experiments using $\bar{H}$ atoms via 1S-2S laser spectroscopy [1, 2] and hyperfine spectroscopy [3, 4].

In 2012, we developed an $\bar{H}$ beam detector consisting of a BGO ($Bi_4Ge_3O_{12}$) calorimeter and 5 plastic scintillator plates. We succeeded in identifying the $\bar{H}$ atoms and confirmed the production of the $\bar{H}$ atomic beams for the hyperfine spectroscopy of the $\bar{H}$ atoms [5]. In the experiment, the count rate of $\bar{H}$ atoms arrived at the beam detector was around 10^{-2} Hz which was much lower than the cosmic ray background of around 1 Hz. To reduce the background, we applied the data cut using the information of the energy deposition in the BGO and the combinations among 5 plastic scintillators detecting charged particles. Although the cosmic ray rejection rate of 99.54% was achieved, the $\bar{H}$ detection efficiency was still 50% [6]. To increase the detection efficiency and improve the efficient rejection of cosmic events, we developed a new $\bar{H}$ beam detector as described below.

©2017 The Author(s)

This article is available under the terms of the Creative Commons Attribution 4.0 License. Any further distribution of this work must maintain attribution to the author(s) and the title of the article, journal citation, and DOI.

Proceedings of the 12th International Conference on Low Energy Antiproton Physics (LEAP2016)
Downloaded from journals.jps.jp by 128.141.46.241 on 03/21/18

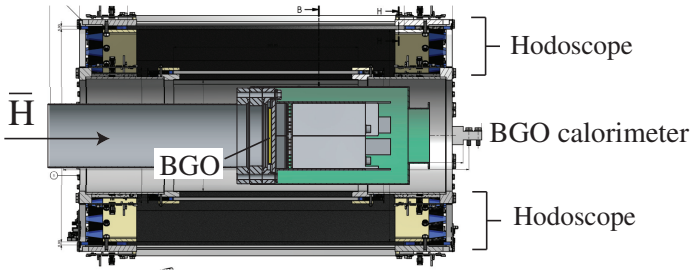

Fig. 1. The $\bar{H}$ beam detector consisting of a position sensitive BGO calorimeter and a hodoscope.

2. $\bar{H}$ beam detector

Figure 1 shows the $\bar{H}$ beam detector consisting of a new BGO calorimeter and a hodoscope. This BGO calorimeter can measure two-dimensional distribution of the energy deposition on the BGO disk. The BGO whose diameter and thickness are 90 mm and 5 mm, respectively, are carbon coated and placed on a viewport glass in UHV. The scintillation light is detected by 4×64ch multi-anode PMTs (MAPMTs: H8500C, Hamamatsu Photonics) through the viewport glass. Output signals of the MAPMT are measured by 4 modules including 64ch amplifiers and charge-to-digital converters (Amp. unit: 80190, Clearpulse).

The hodoscope is placed at around the BGO calorimeter as shown in Fig. 1 to detect charged particle tracks [7, 8]. The hodoscope has two layers of 32 plastic scintillator bars. Silicon photomultipliers (SiPMs) are connected to each scintillator bar on both ends. Pulse shapes from all SiPMs are recorded by 4×32 channel waveform digitizers. The charged particle tracks are reconstructed by connecting the positions of plastic scintillator bars detecting charged particles and the hit position of the charged particle in the BGO calorimeter.

3. Position sensitive readout with non-segmented scintillator

The two-dimensional position sensitive readout of scintillation light is usually achieved by using segmented scintillators with the position sensitive light detector such as a MAPMT, a CCD and a position sensitive SiPM. However, the position readout was not easy technically with the scintillator plate in UHV. If the scintillation light has directivity toward the light detector, the profile measured by the detector can determine the light emission position in two-dimensional plane without the segmentation. Figure 2 shows the conceptual drawing showing the directivity of the scintillation light from the scintillator. The scintillator plate is placed in the vacuum. For higher refraction index n_r of the scintillator, the critical angle θ_c is smaller to make full reflection. For the BGO, $n_r = 2.1$ and $\theta_c = 27$ degrees. The scintillation light emitted from A can pass through the scintillator surface if the incident angle is less than θ_c. If the light is detected by the position sensitive detector, the information of around the position A is obtained. As is clear from Fig. 2, the position resolution is better for a thinner scintillator plate.

To study the position sensitivity of the scintillation light, we performed the test experiment with the setup as shown in Fig. 3. The size of the BGO plate used in this test experiment was 40 mm $\times$ 40 mm with the thickness of 5 mm. This BGO plate was not coated with carbon. The scintillation light was detected by the MAPMT with the coincidence of the signal from the plastic scintillator whose thickness was 10 mm. The MAPMT has 64 anodes (8×8) with one anode of 6 mm $\times$ 6 mm. The 64 channel outputs from the MAPMT were connected to the Amp. unit and were amplified, digitalized, and recorded as 64 charges qs. The total charge Q was obtained by summing up all 64 qs. The plastic scintillator was placed beneath the BGO plate with a PMT (H7195, Hama-

Proceedings of the 12th International Conference on Low Energy Antiproton Physics (LEAP2016)
Downloaded from journals.jps.jp by 128.141.46.241 on 03/21/18

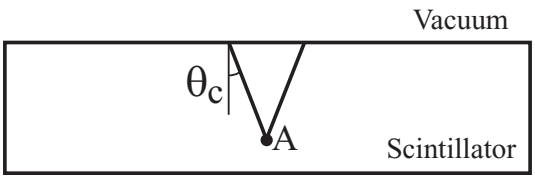

Fig. 2. Conceptual drawing showing the position sensitivity of the scintillation light from the scintillator.

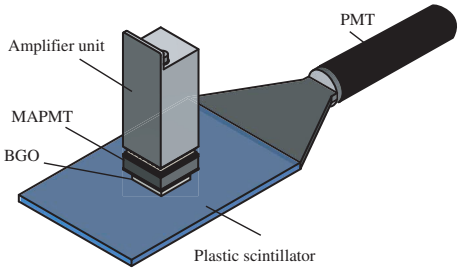

Fig. 3. The setup to study the position sensitivity of the BGO scintillator.

matsu Photonics). Cosmic rays were measured by this BGO-MAPMT with the trigger generated by the coincidence signal of the BGO and the plastic scintillator.

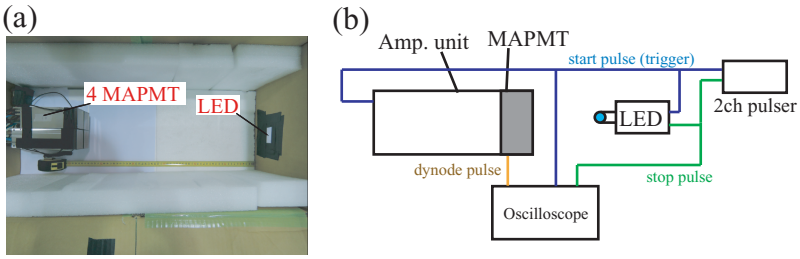

Fig. 4. (a)A photo of the setup for the uniformity calibration with a LED. (b)The schematic drawing of the setup.

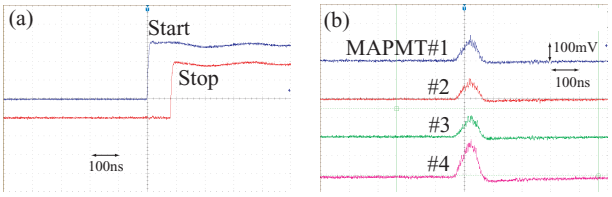

Fig. 5. (a) The LED start and stop pulses. (b) Dynode signals for 4 MAPMTs.

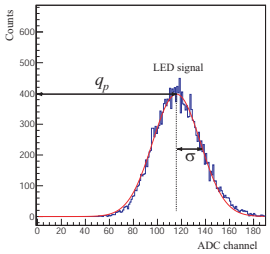

Fig. 6. Example of q distribution for one channel.

The uniformity of the MAPMT was calibrated in advance with an LED flashing on the MAPMT directly. Figure 4 shows a photo and a schematic drawing of the experimental setup, where we placed 4 MAPMTs which were used for the $\bar{\mathrm{H}}$ beam detector. The LED was placed 50 cm apart from the MAPMTs. The LED start and stop signals with the time interval of 80 ns in Fig. 5 (a) were supplied from a two-channel pulse generator. The dynode signals of MAPMTs were measured by the oscilloscope as shown in Fig. 5 (b). Although the same voltages, −1000 V, were applied on all MAPMTs, the obtained charges were different from each other. In order to normalize measured charges to that of an arbitrary selected MAPMT (MAPMT #1 shown in Fig. 5 (b)), voltages applied on other MAPMTs

Proceedings of the 12th International Conference on Low Energy Antiproton Physics (LEAP2016)
Downloaded from journals.jps.jp by 128.141.46.241 on 03/21/18

were adjusted. Then we made a charge map for all channels to calibrate the uniformity. We measured q for each channel with the LED many times and drew the q distribution as shown by the blue histogram in Fig. 6. The red line is a Gaussian fit to the experimental result. The peak position and the standard deviation are labeled as q_p and σ for each channel. Figures 7 (a1)-(a4) are q_p maps normalized to 100 for 4 MAPMTs. For example, in Fig. 7 (a2), the lowest q_p is 37.7, thus the largest difference of q_p is a factor of around 3. The uniformity was calibrated by dividing the data by this map. Figures 7 (b1)-(b4) show the same maps from the company, where the DC light was used for the measurement. We calculated the differences between Figs. 7 (a1) and (b1) divided by (b1), and then made a histogram of those 64 values, and obtained its standard deviation of 4%. Therefore Figs. 7 (a1) and (b1) are in agreement with each other. The maps (a2)-(a4) and (b2)-(b4) also agree well. Figures 7 (c1)-(c4) show σ/q_p maps for 4 MAPMTs normalized to 100. The lowest values of σ/q_p for 4 MAPMTs shown in Figs 7 (c1)-(c4) are 81.3, 85.1, 84.5 and 78.0, respectively. Although the largest q_p difference is a factor of 3, the difference of σ/q_p is only less than 22 %. This fact suggests that if the uniformity is calibrated, the energy resolution is much improved.

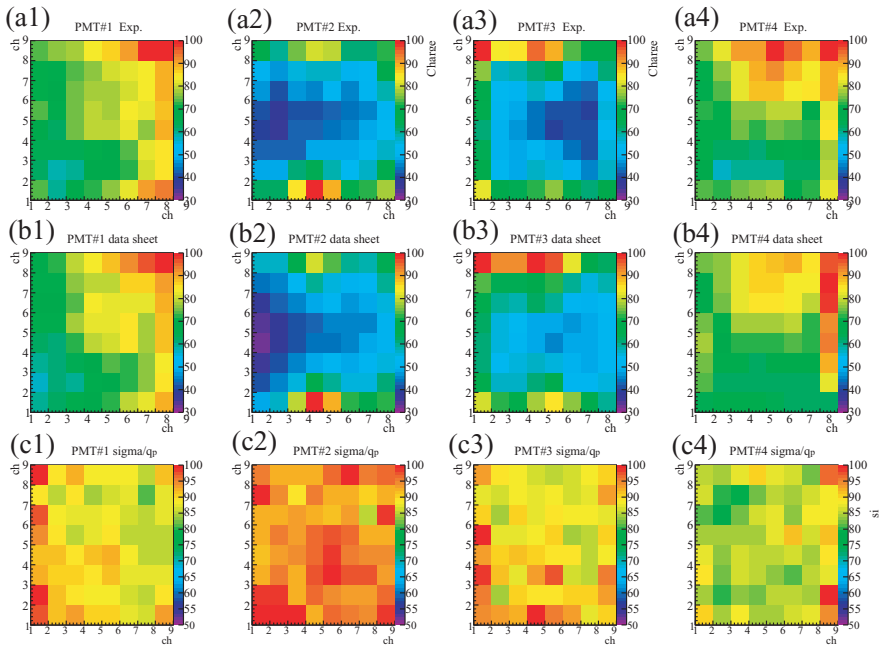

Fig. 7. (a1)-(a4) Charge maps measured for 4 MAPMTs with a LED light. (b1)-(b4) Same but from the data sheet of the company. (c1)-(c4) σ/q_p maps.

We measured cosmic rays for the setup as shown in Fig. 3 to study the position sensitive readout, where MAPMT#1 was used. Figure 8 (a1) shows the BGO setup. Figure 8 (b1) shows the charge map obtained by the sum of qs for 46 cosmic ray events having a maximum charge on the channel A (back view) for the setups of (a1). The thick black line shows the outline of the BGO plate. Photons are detected along the edge of the BGO. Figure 8 (c1) and (d1) are x and y projections, respectively, where we analyzed for the channels inside the red dotted line in Fig. 8 (b1) to remove the light along the edge of the BGO. The blue histograms are experimental data. We defined the background of the data as the average of ch3 and ch7 for (c1), or ch2 and ch6 for (d1). The backgrounds were around 700. The red line shows the Gaussian fit to the experimental data. The standard deviations σ_x and σ_y were 6.4 mm for (c1) and 6.6 mm for (d1), respectively. To reduce the light along the edge of the BGO, we taped the side of the BGO by the black tape as shown in Fig. 8 (a2). The light

Proceedings of the 12th International Conference on Low Energy Antiproton Physics (LEAP2016)
Downloaded from journals.jps.jp by 128.141.46.241 on 03/21/18

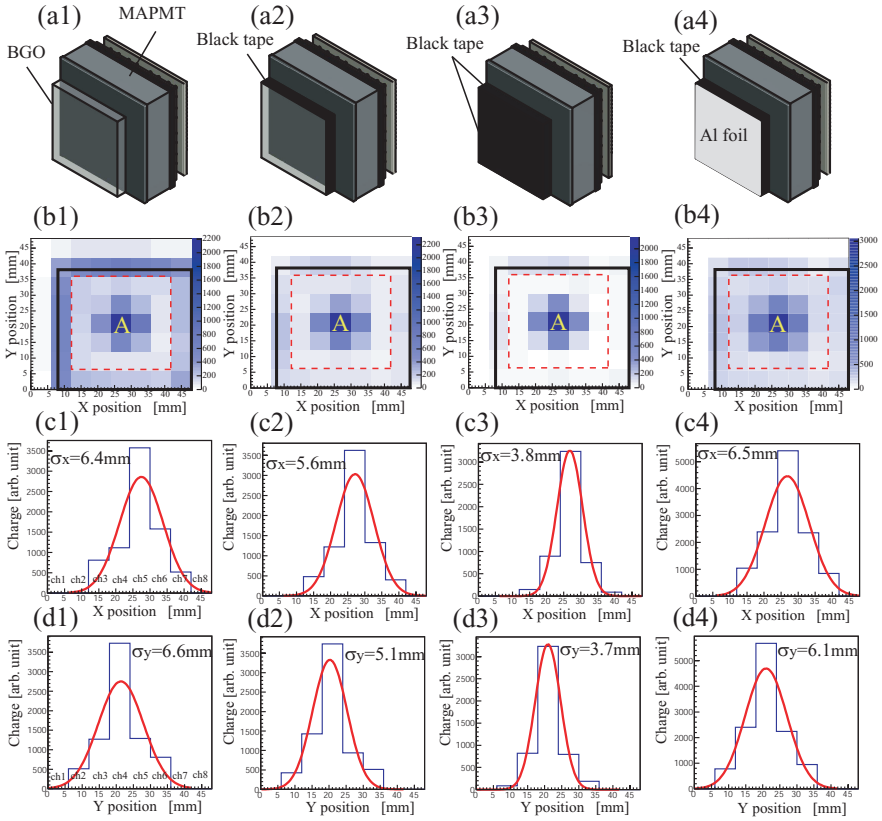

Fig. 8. (a1)-(a4) show the setups of the BGO. (b1)-(b4) show charge maps obtained by the sum of 46 cosmic ray events having a maximum charge on the channel A (back view). (c1)-(c4) and (d1)-(d4) are x and y projections, respectively.

was considerably reduced as shown in Fig. 8 (b2). The background and the peak value were not so changed. Those standard deviations σ_x and σ_y were 5.6 mm and 5.1 mm, respectively. To further reduce the background, we taped the front of the BGO by the black tape as shown in Fig. 8 (a3). The background was reduced to around 150, although the peak value still kept 90 % of the case without black tapes. The standard deviations σ_x and σ_y were 3.8 mm and 3.7 mm, respectively. Figure 8 (a4) shows the setup with the aluminum foil on the surface of the BGO and the black tape on the side of the BGO. The peak value and the background increased to 5400 and 1000, respectively. The standard deviations σ_x and σ_y were 6.5 mm and 6.1 mm, respectively. Although, in this case, the scintillation light was collected efficiently, σ_x, σ_y and the ratio of the peak value to the background were worse than other setups. Therefore the setup (a3) was the best among these setups.

For the application of $\bar{\mathrm{H}}$ detection, the scintillation light is collected through the viewport glass. In order to study this effect, we inserted a glass plate of 40 mm $\times$ 40 mm and 4 mm thickness between the MAPMT and the BGO for the setup shown in Fig. 8 (a3) with black tapes and measured the cosmic rays. Figures 9 (a) and (b) show x and y projections where the analysis condition was the same as Figs. 8 (c3) and (d3). The backgrounds were similar to Figs. 8 (c3) and (d3). The standard deviations σ_x and σ_y were 5.1 mm and 4.9 mm, respectively. These values were slightly larger than Figs. 8 (c3) and (d3) but still less than the MAPMT channel size, and hence are acceptable for the measurement of two-dimensional distribution of the energy deposition. In these experiments, σ_x and σ_y do not mean the position resolution and become larger than it, because the comic rays with various incident directions are distributed in A.

Proceedings of the 12th International Conference on Low Energy Antiproton Physics (LEAP2016)
Downloaded from journals.jps.jp by 128.141.46.241 on 03/21/18

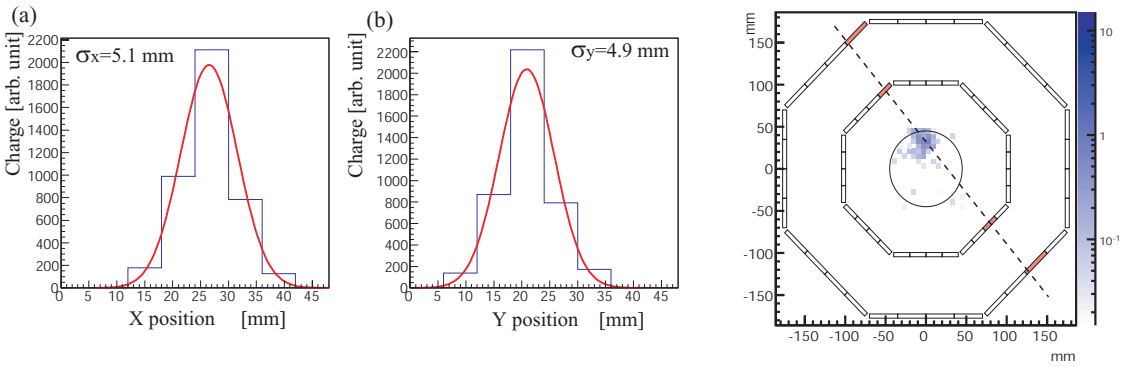

Fig. 9. The x and y projections with a glass plate of 4 mm thickness which was inserted between the MAPMT and the BGO for the setup shown in Fig. 8 (a3). The analysis is the same as Figs. 8 (c3) and (d3).

Fig. 10. Example of the cosmic ray event.

4. Cosmic ray event measured by the $\bar{H}$ beam detector

Figure 10 shows the example of the cosmic ray event measured by the $\bar{H}$ beam detector. The BGO calorimeter shown by the center circle, measured one hit position. The hodoscope measured the signals for 4 scintillator bars as shown by the red color boxes. The track of the cosmic ray event can be found as shown in Fig. 10. The detector showed the capability to reconstruct cosmic ray events.

5. Summary

We reported the test experiments for the position sensitive readout from the non-segmented BGO scintillator. In this test, the uniformity of the MAPMT was calibrated with the LED light. The position sensitivity was evaluated with the cosmic rays for various setups using black tapes, aluminum foils and the glass spacer. The best setup for the position sensitivity was obtained utilizing black tapes. We developed the $\bar{H}$ beam detector consisting of the position sensitive BGO calorimeter and the hodoscope for the measurement of $\bar{H}$ atomic beams. The $\bar{H}$ beam detector was tested with cosmic rays.

Acknowledgements

This work was supported by the Grant-in-Aid for Specially Promoted Research (19002004 and 24000008) of Japanese Ministry of Education, Culture, Sports, Science and Technology (MEXT), Special Research Projects for Basic Science of RIKEN, RIKEN FPR program, RIKEN IRU program, European Research Council under European Union's Seventh Framework Programme (FP7/2007.2013) / ERC Grant agreement (291242), the Austrian Ministry for Science and Research, Università di Brescia, and Instituto Nazionale di Fisica Nucleare.

References

[1] G. B. Andresen et al: Nature **468** (2010) 673.
[2] G. Gabrielse et al: Phys. Rev. Lett. **108** (2012) 113002.
[3] Y Yamazaki and S Ulmer: Ann. Physik **525** (2013) 493.
[4] B. Juhász and E. Widmann : Hyperfine Interact **193** (2009) 305.
[5] N. Kuroda et al: Nat. Commun. **5** (2014) 3089.
[6] Y. Nagata and N. Kuroda et al: Nucl. Instrum. Methods Phys. Res. Sect. A **840** (2016) 153.
[7] C. Sauerzopf et al: Nucl. Instrum. Methods Phys. Res. Sect. A, **819** (2016) 163.
[8] C. Sauerzopf et al: Nucl. Instrum. Methods Phys. Res. Sect. A, **845** (2016) 579.